STUDY THE NEAR PLANE STRAIN TENSILE TEST SPECIMEN USING FINITE ELEMENT CODE ABAQUS

Meknassi Raid Fekhreddine
PhD student, University of Miskolc, Institute of Mechanical Engineering and information, Department of Mechanical Technologies
3515 Miskolc, Miskolc-Egyetemváros, e-mail: metraid@uni-miskolc.hu

Gábor Béres
senior lecturer, John von Neumann University, GAMF Faculty of Engineering and Computer Science, Kecskemét, Hungary, e-mail: beres.gabor@gamf.uni-neumann.hu

Zsolt Lukács
associate professor, University of Miskolc, Institute of Materials Science and Engineering, Department of Mechanical Technologies
3515 Miskolc, Miskolc-Egyetemváros, e-mail: zsolt.lukacs@uni-miskolc.hu

Abstract
In the present work, optimization of near plane strain tensile test specimen for four types of cold-rolled steel DC01, DC04, DP600, and DP1000 are studied using finite element code ABAQUS. The sample width (A), notch radius (R), and material anisotropy (r-value) were the main parameters considered in this study. The effects of these parameters on the Plane Strain State Index (PSSI) and Homogeneity Index (HI) were analyzed and presented.

Keywords: *tensile test, plane strain, FE method, FLC*

1. Introduction

In sheet metal forming, the accurate predicting of the material behaviors during straining is associated directly with the correct understanding of locating the yield point damage and strain distribution (Münstermann et al., 2012). Forming Limit Diagram (FLD), sometimes called the Keeler and Goodwin diagram after its developers, is considered the most used prediction tool for defining the failure criteria in sheet metal forming (Keeler et al., 1964; Goodwin et al., 1968). FLD is usually obtained through the Nakajima and Marciniak tests according to the ISO 12004-2:2008 standard (Marciniak, 1967; IOS, 2008). Various studies showed that this test is sensitive to many factors such as the sheet thickness, lubricants, complexity of tools and geometry shape, Etc. (Banabic, 2000; Laukonis et al., 1978; Rees, 2001). Also, the excessive number of required samples made the test time-consuming and expensive.

Many research papers have been conducted and brought new solution ideas to overcome the path-independent problem. Xavier (Xavier, 2014) evaluated the possibility of replacing Nakajima tests with a fast and safe determination of the FLC0 value through tensile tests, which corresponds to the minimum (lowest point) of the FLC curve under plane strain. He was able with his test to reach near plane strain deformation using a smaller number of samples. Saxena (Saxena, 2015), developed a novel experimental approach for detecting forming limits considering non-linear strain paths using new modified punch geometry. She obtained the FLD for applying two deformations modes from the same punch, employing first induce the bending which causes the plain strain, then the stretching shifts it to the biaxial region.

In our work, we intend to optimize a sample geometry for the plane strain tensile test that could allow us to apply another deformation test, which eventually leads to determining the forming limits diagram path-independent. The used sample dimensions were based on Wagoner’s previous studies (Wagoner, 1980). A finite element code, ABAQUS used to study the strain behavior and measure the effects of sample width (*A*), notch radius (*R*), and the material anisotropy (*r-value*) on the Plane Strain State Index (PSSI) and Homogeneity Index (HI) using four types of cold-rolled steel DC01, DC04, DP600, and DP1000.

2. Material and method

2.1. Material and sample geometry

We considered 1 mm thickness for all the test samples and four cold-rolled steel materials in our investigation. The geometries of the samples used are shown in Figure 1, and our measured mechanical properties parallel, perpendicular and 45°to the rolling direction are given in Table 1 (Wagoner et al., 1980).

To study the effect of various parameters (A, *R*, *r-value*) on the strain field distributions, the factors and their levels are presented in Table 2. The values chosen are as follows: sample width *A* (60, 80, and 100 mm), notch radius *R* (10, 11, and 12 mm), and the material anisotropy *r* (0.76, 0.92, 1.99, and 1.7).

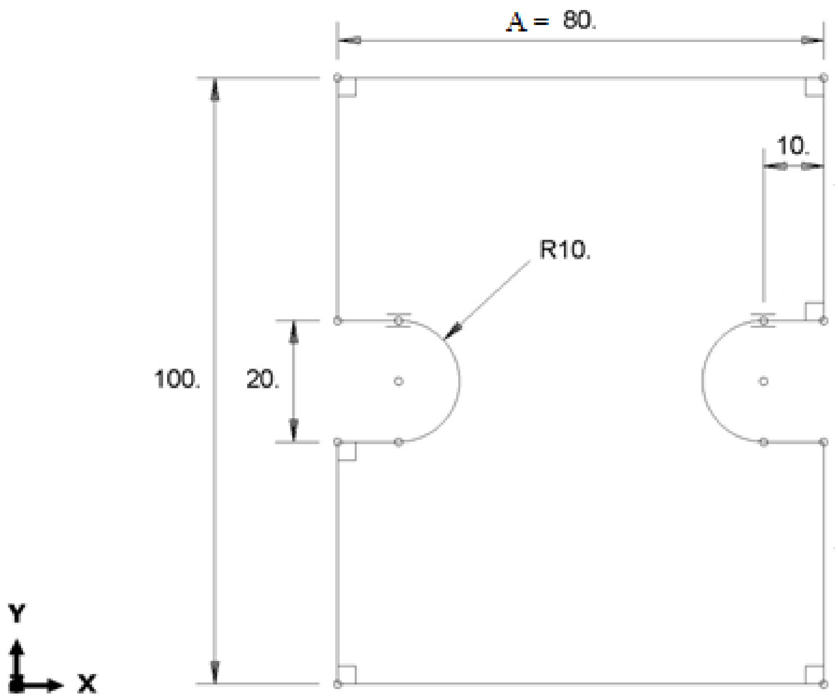

Figure 1. *Sample geometry, used in the plane strain tensile test simulation*

Table 1. *Data for yield parameters of all four material*

	Orientation angle	A_{80} (%)	A_{80_ave} (%)	*r*	$\bar{r}$	*Δr*	$Rp_{0,2}$ (N/mm^2)	$Rp_{0,2\_ave}$ (N/mm^2)	R_m (N/mm^2)	R_{m_ave} (N/mm^2)
DC01	0°	40,0	38,0	2,35	1.99	0,88	199	201	306	309
	45°	36,0		1,55			206		322	
	90°	39,0		2,52			198		298	
DC04	0°	41,0	37,9	1,94	1,7	0,10	230	238	328	336
	45°	35,4		2,05			240		346	
	90°	39,6		2,18			240		325	
DP600	0°	21,6	20,6	0,80	0,92	0,01	434	444	645	656
	45°	20,5		0,91			441		655	
	90°	19,8		1,12			461		669	
DP1000	0°	11,7	10,6	0,74	0,76	0,05	781	758	1099	1099
	45°	10,5		0,71			732		1087	
	90°	9,7		0,79			789		1111	

Where: A80 is the total engineering strain, A80_ave is the average total engineering strain, r is the r-value, $\bar{r} = \frac{(r0+r90+2\,.r45)}{4}$ is the normal anisotropy, $\Delta r = \frac{(r0+r90)}{2-r45}$ is the planar anisotropy, $Rp_{0,2}$ is the yield strength, $Rp_{0,2\_ave}$ is the average yield strength, Rm is the tensile strength and R_{m_avr} is the average tensile strength.

Table 2. *Factors and their levels for the tests*

Control parameters	Unite	Symbol	Levels			
			Level 1	Level 2	Level 3	Level 4
Sample width	mm	*A*	60	80	100	/
Notch radius	mm	*R*	10	11	12	/
r-value	/	*r*	1,99	1,7	0,92	0,76

For comparison of the different specimen geometries responses, we used the following equations:

- Plane strain state index (*PSSI*): the closer the average minor strain ($A_{\varepsilon 2}$) to zero, the better it is

$$PSSI = A_{\varepsilon 2} = \frac{\sum_{i=1}^{n} \varepsilon_2}{n} \quad (n = 1 \dots 9). \tag{1}$$

- Homogeneity index (*HI*) (equivalent with standard deviation): the smaller the *HI*, the better is the result

$$HI = \sqrt{\frac{\sum_{i=1}^{n}(\varepsilon_1^n - A_{\varepsilon 1})^2}{n}} \quad (n = 1 \dots 9). \tag{2}$$

2.2. Finite element modelling

The code used for simulation is Abaqus 2021, with Hill (1948) yield criterion developed by Hill (1948) (Eq. (3), written in terms of the Lankford coefficients r), and by defining the six plastic potentials R11, R22, R33, R12, R13, R23 could be calculated using these equations (4, to 7) (Safdarian, 2015). Table 3. shows the analytical results we used as an inputs parameter in our software. In order to calculate the plastic stress-strain behavior of the investigated materials, the Swift non-linear isotropic hardening model, shown in equation (8), was used with our measured data shown in Table 4.

All specimens have a 30 mm griping area length on both sides and 0.8 mm mesh size of a three-dimensional eight-node brick element with six integration points is used. The boundary and loading conditions are applied in a manner that is as similar to the real tensile test experiment as possible. The lower grip of the specimen was kept fixed in all directions but free in the direction of the applied load. The sliding between grips and specimen is neglected. The maximum major and minor strain values are extracted in the strain hardening region before the local cross-sectional area becomes significantly smaller than the average (necking region). The data gathered from nine points in the middle area of all samples were, as shown in Figure 2

$$\Phi(\sigma) = \frac{r_{TD}(r_{RD}+1)\sigma_{11}^2 + r_{RD}(r_{TD}+1)\sigma_{22}^2 - 2r_{RD}r_{TD}\sigma_{11}\sigma_{22} + (r_{RD}+r_{TD})(2r_{45^\circ}+1)\sigma_{11}^2}{r_{TD}(r_{RD}+1)} - \bar{\sigma} = 0; \tag{3}$$

$$R_{11} = R_{13} = R_{23} = 1; \tag{4}$$

$$R_{22} = \sqrt{\frac{r_{90}\,(r_0+1)}{r_0\,(r_{90}+1)}}; \tag{5}$$

$$R_{33} = \sqrt{\frac{r_{90}\,(r_0+1)}{r_0 + r_{90}}}; \tag{6}$$

$$R_{12} = \sqrt{\frac{3r_{90}\,(r_0+1)}{(2r_{45}+1)\,(r_0+r_{90})}}; \tag{7}$$

$$\bar{\sigma} = K(\varphi_0 + \bar{\varphi})^n\,. \tag{8}$$

Here, $\bar{\sigma}$, $\bar{\varphi}$, are respectively the current yield stress and anisotropic equivalent plastic strain. Hardening is defined by the material parameters K, *n* and φ_0.

Table 3. *Analytical calculation results for Hill 48 plastic potentials*

	R11	*R22*	*R33*	*R12*	*R13*	*R23*
DC01	1.00	1.01	1.32	1.13	1.00	1.00
DC04	1.00	1.02	1.25	0.96	1.00	1.00
DP600	1.00	1.09	1.025	1.06	1.00	1.00
DP1000	1.00	1.09	0.95	1.05	1.00	1.00

Table 4. *Swift equation data for the used materials*

Material	**Swift equation**		
	K [MPa]	φ_0 **[-]**	***n*** **[-]**
DC01	578	0.0173	0.220
DC04	578	0.0173	0.220
DP600	1044	0.0046	0.16
DP1000	1578	0.0005	0.098

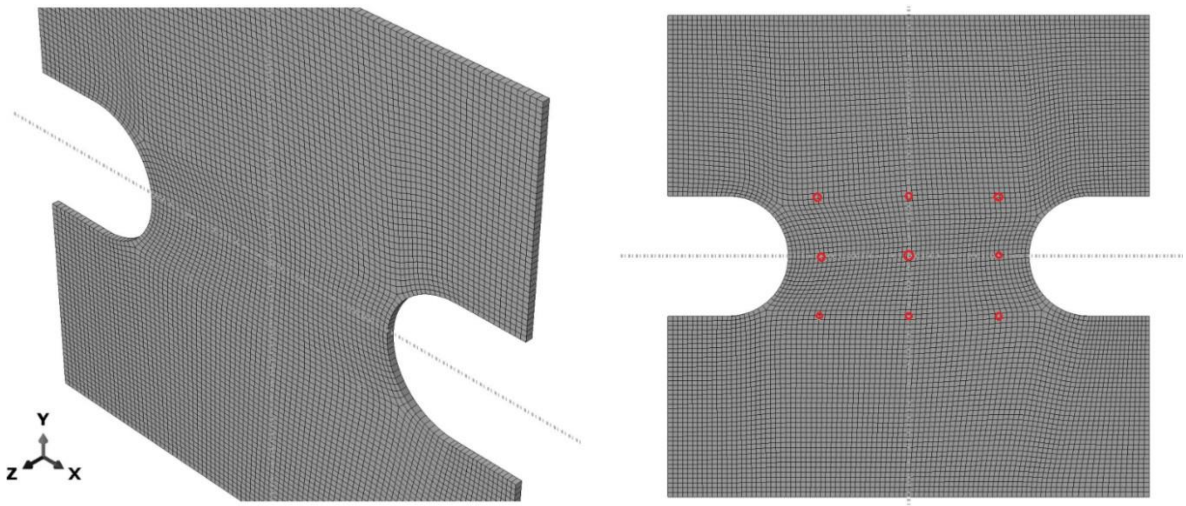

Figure 2. *Mesh and data points of the standard geometry*

3. Results and discussion

The results of the investigation are summarized in Tables 5 and 6. Figures 3 and 4 present results for the evolution of HI and PSSI depending on the different parameters (A, R, and r-value).

Figure 3.a and 3.b shows the evolution of the responses PSSI and HI as a function of the sample width (A). When the A increases from 60 to 100 mm, we can see a significant decrease in HI on the one hand and an increase in PSSI on the other. This proves that in this interval, the notch angle has a significant influence on the plan strain distribution and Homogeneity Index. From a practical point of view, the wider specimen compared to the length gives a more extensive necking area, eventually leading to a better near-plan strain deformation.

Figures 4.a and 4.b describes the evolution of the PSSI and HI criteria as a function of notch radius (R). Unlike the previous geometries, it is noted that the PSSI values decreased while HI showed a significant increase. It could be explained that in the range of 10 to 12 mm, the notch radius has a remarkable effect on the plane strain tensile test.

Figures 5.a and 5.b illustrate the r-value (r) effect on the PSSI and HI. There is an apparent deterioration in both PSSI and HI at the same time as the anisotropy increases. It is easy to see that (r) plays a crucial role in strain distribution during the plane strain tensile test.

Table 5. *Summary of parametric study results for A*

A (mm)	**PSSI max**				**HI max**			
	DC01	**DC04**	**DP600**	**DP1000**	**DC01**	**DC04**	**DP600**	**DP1000**
60	-0.0782	-0.0714	-0.0294	-0.0256	0.397	0.3836	0.2807	0.2513
80	-0.0718	-0.0434	-0.0111	-0.0094	0.2168	0.1406	0.1394	0.0996
100	-0.0279	-0.0245	-0.0088	-0.0053	0.0856	0.0819	0.0529	0.0397

Table 6. *Summary of parametric study results for R*

R (mm)	**PSSI max**				**HI max**			
	DC01	**DC04**	**DP600**	**DP1000**	**DC01**	**DC04**	**DP600**	**DP1000**
10	- 0.0388	-0.0252	-0.0102	-0.0100	0.12	0.0835	0.0717	0.0611
11	-0.0725	-0.0414	-0.0144	-0.0910	0.1907	0.117	0.0811	0.0795
12	-0.0738	-0.0434	-0.0172	-0.0094	0.2168	0.1406	0.1395	0.0996

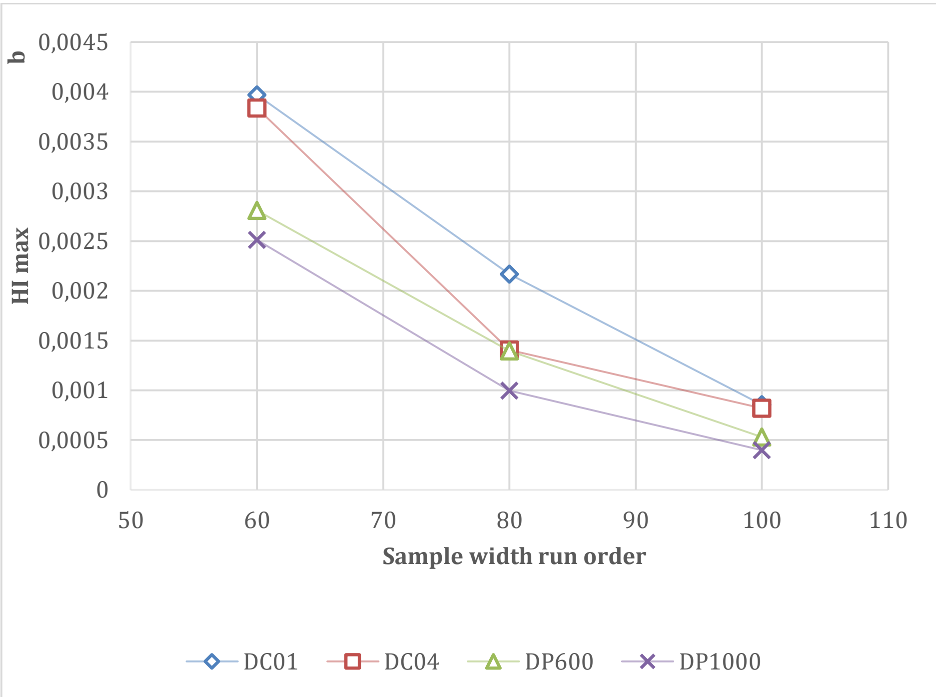

Figure 3. *Effect of the sample width on PSSI and HI*

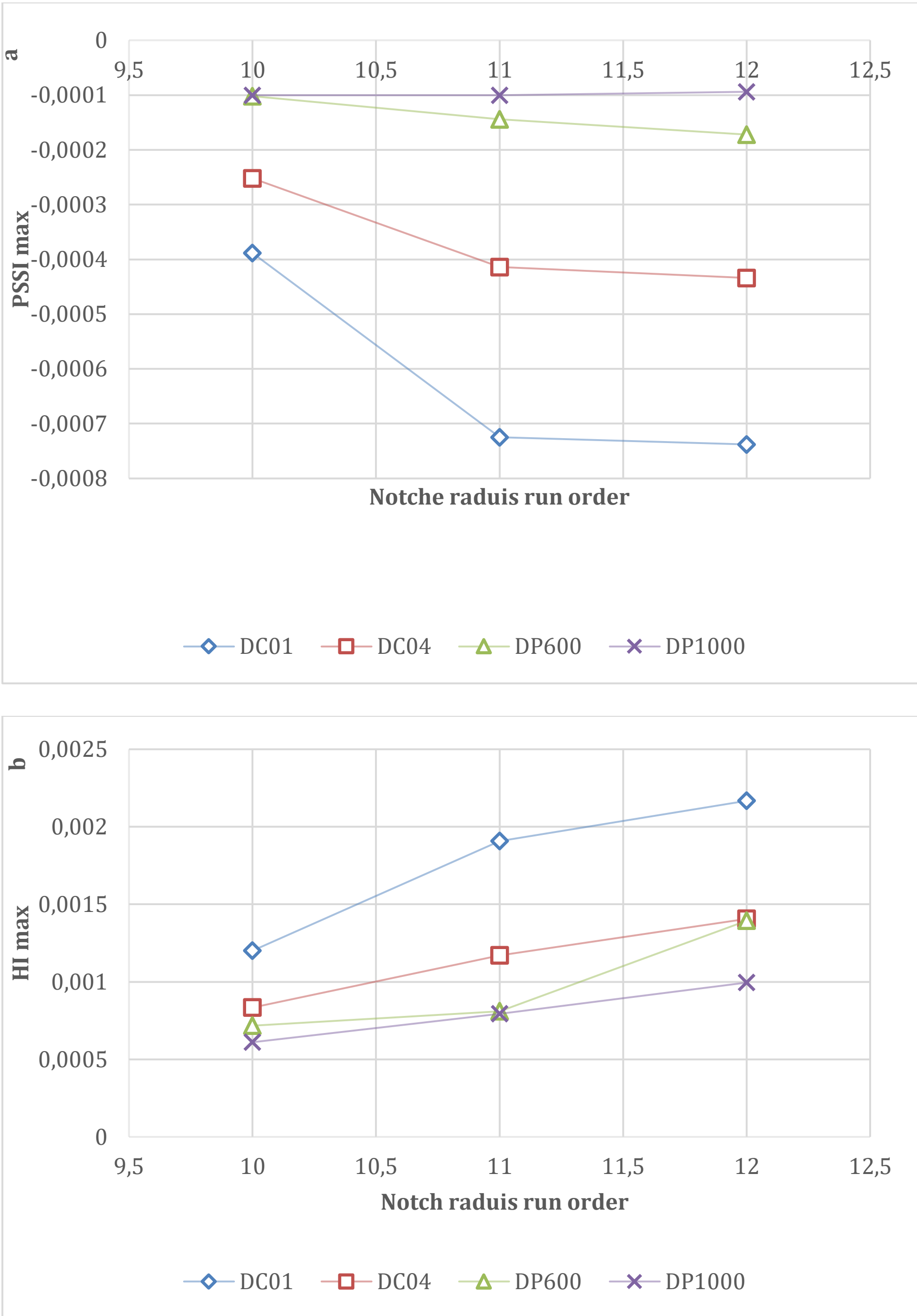

Figure 4. *Effect of the notch raduis on PSSI and HI*

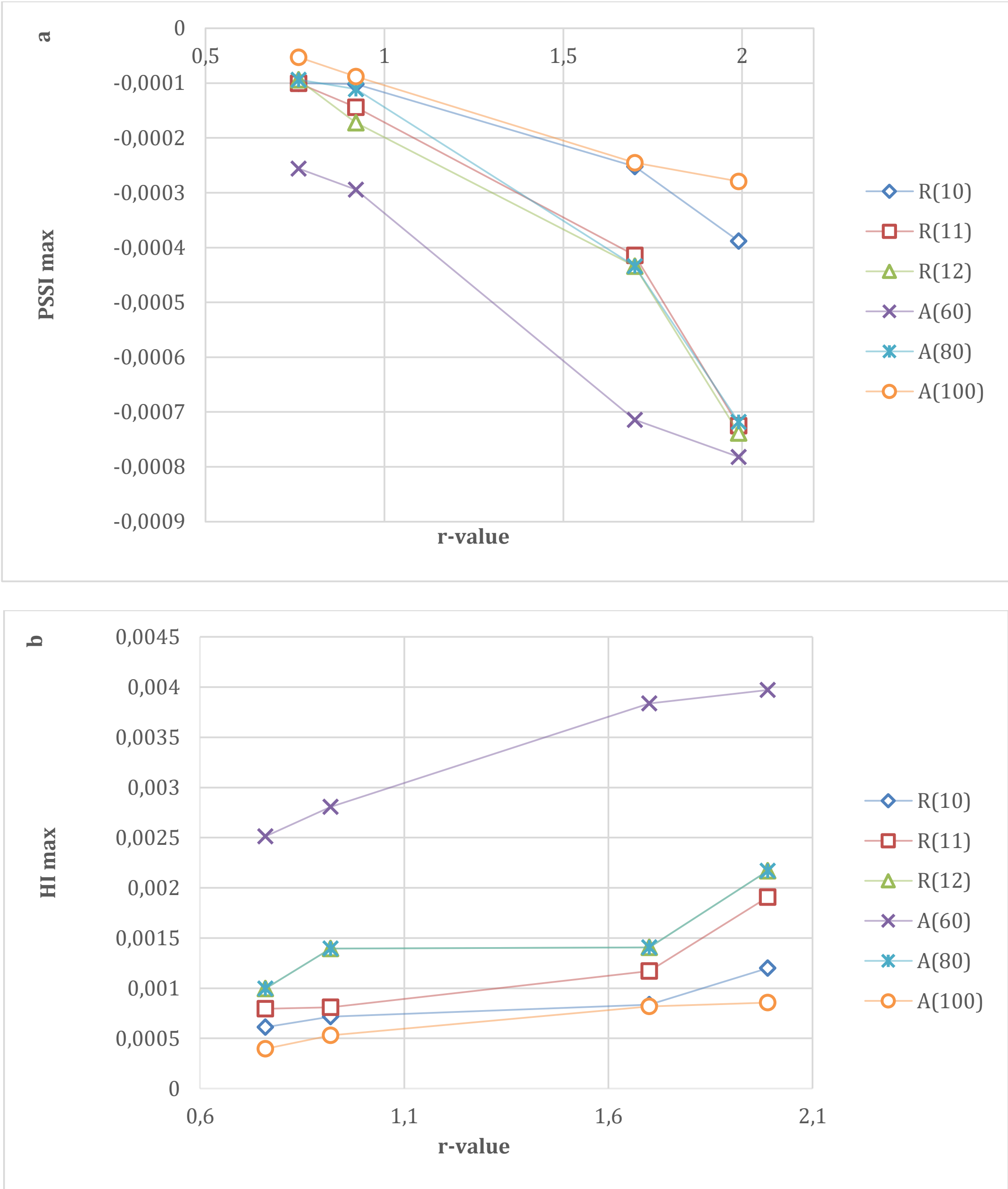

Figure 5. *Effect of the r-value on PSSI and HI*

4. Summary

The investigation results showed that the specimen width is a very important parameter influencing PSSI and HI. Moreover, increasing the notch radius was unfavorable for the plane strain tensile test and must be avoided. The comparison between the four materials showed that the r-value should be considered during the test, where the preferred *r* value in the range of our test {0,76 to1,7} is 0,76.

References

[1] Münstermann, S., Lian, J., and Bleck, W. (2012). Design of damage tolerance in high-strength steels. *International Journal of Materials Research*, 103(6), 755–764. **https://doi.org/10.3139/146.110697**

[2] Keeler, S. P., and Backofen, W.A. (1964). Plastic instability in sheet stretched over rigid punches. *ASM Transactions Quarterly*, 56(11), 25–48.

[3] Good win, G. (1968). *Application of strain analysis to sheet metal forming problems in the press shop*. SAE Technical Paper. (680093) **https://doi.org/10.4271/680093**

[4] Zdzislaw, M., and Kuczyński, K. (1967). Limit strains in the processes of stretch-forming sheet metal. *International Journal of Mechanical Sciences*, 9(9), 609–620. **https://doi.org/10.1016/0020-7403(67)90066-5**

[5] International Organization for Standardization. (2008). ISO/DIS 12004-2: 2008. Metallic Materials–Sheet and Strip–Determination of Forming Limit Curves–Part 2: Deformination of Forming limit Curves in the Laboratory.

[6] Banabic, D. (2000). Forming limits of sheet metal. In *Formability of metallic materials: plastic anisotropy*, *formability testing*, *forming limit*. Berlin: Springer Verlag; p. 173–214. **https://doi.org/10.1007/978-3-662-04013-3_5**

[7] Laukonis, J.V., and Ghosh, A. K. (1978). Effect of strain path changes on the formability of sheet metals. *Metallurgical Transactions A*, 9(12), 1849–1856. **https://doi.org/10.1007/BF02663419**

[8] Rees, D. W. A. (2001). Factors influencing the FLD of automotive sheet metal. *Journal of Materials Processing Technology*, 118(1-3), 1-8. **https://doi.org/10.1016/S0924-0136(01)01030-5**

[9] Xavier, M. D. (2014). Uniaxial near plane strain tensile tests applied to the determination of the FLC0 formabillity parameter. *Materials Research*, 17, 982–986. **https://doi.org/10.1590/S1516-14392014005000083**

[10] Saxena, K. (2015). *A novel experimental approach for detection of forming limits considering non linear strain paths*.

[11] Wagoner, R. H. (1980). Measurement and analysis of plane-strain work hardening. *Metallurgical and Materials Transactions A*, 11(1), 165–175. **https://doi.org/10.1007/BF02700453**

[12] Safdarian, R. (2015). A comparative study of forming limit diagram prediction of tailor welded blanks. *International Journal of Material Forming*, 8(2), 293–304. **https://doi.org/10.1007/s12289-014-1168-9**